Bull. Astr. Soc. India (1993) **21,** 103-123

H_α, microwave and hard X-ray observations of the two-ribbon flare of 1980 April 3

Rajmal Jain

Udaipur Solar Observatory (Physical Research Laboratory, Department of Space, Govt of India), 11, Vidya Marg, Udaipur 313 001

Received 1992 August 14, accepted 1993 January 25

Abstract. The H_α observations of a class 2B two ribbon flare, associated with exceptional hard X-ray and microwave emissions, are presented and discussed. The observational relationship suggests that gradient of magnetic field plays a role in governing the magnitudes of MW and HXR emissions. From the analysis of MW emissions in view of H_α flare kernels, it is concluded that there were two sources for MW emissions and both were moving away from each other. Further, it is also concluded that either two mechanisms were simultaneously operating or double injection of energetic electrons at two different heights was taking place. The energetics and dynamics are derived on the basis of thermal and non-thermal models. The parameters deduced from them suggest that same electron population produced HXR and MW emissions at a frequency near the peak frequency, and that the flare event may be explained by both thermal and non-thermal incidence. Further, the most energetic part of this extended flare is identified which was associated with strong HXR and MW bursts. This part was tested for coronal trap and precipitation model in view of thick target and thin target cases. On the basis of T_{eff}, it was found that the precipitation model corresponding to thick target case is suitable for the production of hard X-rays and microwave emissions, however, the possibility for trap-plus-precipitation model also exists.

Key words : H-alpha—solar flare—thick target—thin target

1. Introduction

The two ribbon flares tend to occur primarily in magnetically complex active regions. The two bright flare ribbons separate with velocities of the order of 1 to 50 km s^{-1}. The velocity is either constant or decreases during the later phase of the flare development (Svestka 1976; Martin 1979; Jain 1983). The complex groups also produce the most energetic flares, giving rise to hard X-rays and radio bursts (Svestka & Simon 1969; de Jager 1975; Jain 1983). The

locations of the hard X-ray burst coincide in position with H_α flare kernels (Hoyng *et al.* 1981). The magnitude of the H_α, X-ray and microwave emission parameters are observed to vary from one flare to another flare according to the location of flares within the active region. This suggests that the strength and configuration of the magnetic field plays a role in governing the flare's emissions (Neiding 1978; Jain 1985). Further, according to Jain (1985), all H_α two ribbon or multi-ribbon flares are not proton or cosmic ray flares but on the other hand all energetic particle events were found associated with two-ribbon or multi ribbon H_α flares. Jain (1986) showed that about 80% of class 3 importance H-alpha two ribbon flares are proton flares.

In the present paper a detailed description of the optical flare of importance 2B which occurred on 1980 April 3 at 0650 UT in Hale active region no. 16740 (N29 W17) is presented. This flare was observed during SMM period and the Hale region 16740 was extensively observed by SMM and ground observatories. The observations of flare associated X-rays, microwave and dynamic radio burst are presented in section 2. In section 3 we give energetics and dynamics of the flare.

2. Observations and analysis

2.1. *Optical observations*

2.1.1. H_α Morphology

The 1980 April 3 flare occurred in the Hale active region 16740 of BY character (Mount Wilson Classification) at 0650 UT. The time lapse observations were made at 10s intervals from the Udaipur Solar Observatory, using the 150 mm aperture telescope, in conjunction with a 0.5A passband Halle filter. During the observations, the solar "seeing" remained between 2-3 arc sec. The Hale active region 16740 appeared on 1980 March 26 on the east limb. It produced many energetic flares. Among these flares, the important flares were of 1980 March 28 which produced unusual inverted 'U' shape type II radio burst (Markeev *et al.* 1983); 1980 March 29 which gave rise to a gamma ray burst; 1980 April 3 which produced MW burst of about 10^3 sfu, and 1980 April 7 flare with the expanding loop which produced a coronal transient on the west limb. In this paper we describe the two-ribbon (TR) flare of 1980 April 3. For this purpose a brief history of this region from 1980 April 1 through April 3, is given in view of the changes which occurred prior to and during TR-flare under study.

Shown in figure 1 are H_α filtergrams of the active region on 1980 April 1st and 2nd. The broken and curvilinear filament F appeared crossing the plage north-south in the region, showed considerable activity throughout the period of observations from 0800 through 1235 UT on April 1 (figure 1 a, b, c, d). The filament material ejected out in the north-east direction. The filament activity is obvious in off band pictures and shown in figure 1 (b, c, d). On April 2, filament motion at the north-east end, subflares and extension of the plage were observed. The north-east end portion of the filament F ejected out around 1000 UT. The observations of the region were taken from 0230 UT to 1200 UT on 1980 April 2.

On 1980 April 3 the observations of the region were taken from 0210 to 0826 UT. In figures 2 and 3, we have shown a few H_α filtergrams of April 3 flares during our observational interval between 0437-0640 and 0647-0810 UT respectively. At 0325 UT, only SW curved portion of the filament F (figure 2a) was visible. At this time, the plage in the region was

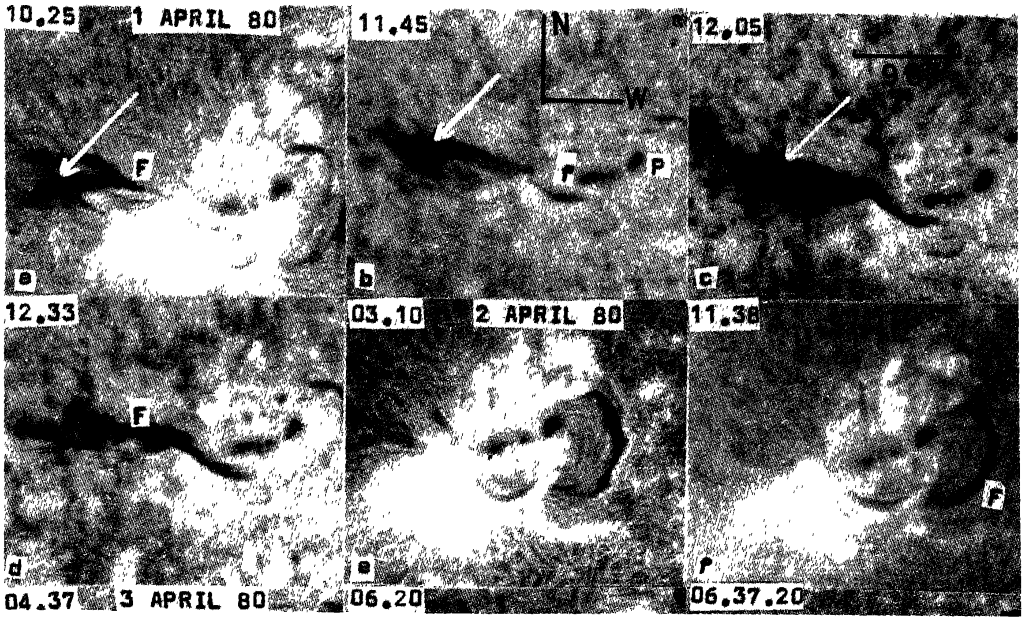

Figure 1. High resolution H_α filtergrams of the Hale region 16740 on 1 and 2 April 1980. The activity in the filament, F, is obvious in off band (H_α – 0.5Å) pictures (b, c, d).

neither intense nor extended, but around 0430 UT the plage expanded and started to become brighter in the region east of the following spot **f**, as shown in figure 2a. During our observations since 0430 UT, we observed discrete dark material shown in figure 2a, b and c by arrow moving from north to south end with a velocity of about 15 km s^{-1} along the loop trajectory below the main curved SW filament **F** (figure 2a). This was observed until the end of the observations. From 0600 UT reorganisation in the field was taking place. Around 0601 UT fine dark fibrils like arches, were observed near spots and extending from preceding to following spots and at different locations in the southern region. The filament **F1**, fine and broken (figure 2b), showed considerable activity since 0525 UT and blown off around 0629 UT. Around 0630 UT a flare of importance 1B occurred in the region and spread over the filament position (figure 2f, g, h). Before this flare completely decayed, it again developed into a second flare of two ribbon type at 0650 UT. The second flare which is the main flare under study was of importance 2B and peaked around 0710 UT (figure 3). The dark filament **F1** was again clearly visible after 0645 UT (figure 3b). The flare ribbons formed on both sides of **F1** were separating away from each other and the dark filament was seen to be reappearing. Before (figure 3a) and during the decay phase of the main flare a new dark fine arch **F2** extending from the preceding to the following spot and north of **F1** was visible. This was also the line of demarcation between various kernels as shown in figure 4b. Figure 4 is a line drawing of the H_α field topology before and after the flare.

A bright mass ejected around 0632 UT was observed to move initially with projected velocity of 60 km s^{-1} which increased to 330 km s^{-1} at about 0639 UT. During the flare activity, dark and bright surges were observed to eject out from the region towards the north-west of the spots (figure 3a, c, f, g).

The full disk magnetogram of this region taken at Mt. Wilson on 1980 April 3 at 1729 UT, obviously about 11 hrs after the flare onset, was published in Solar & Geophysical

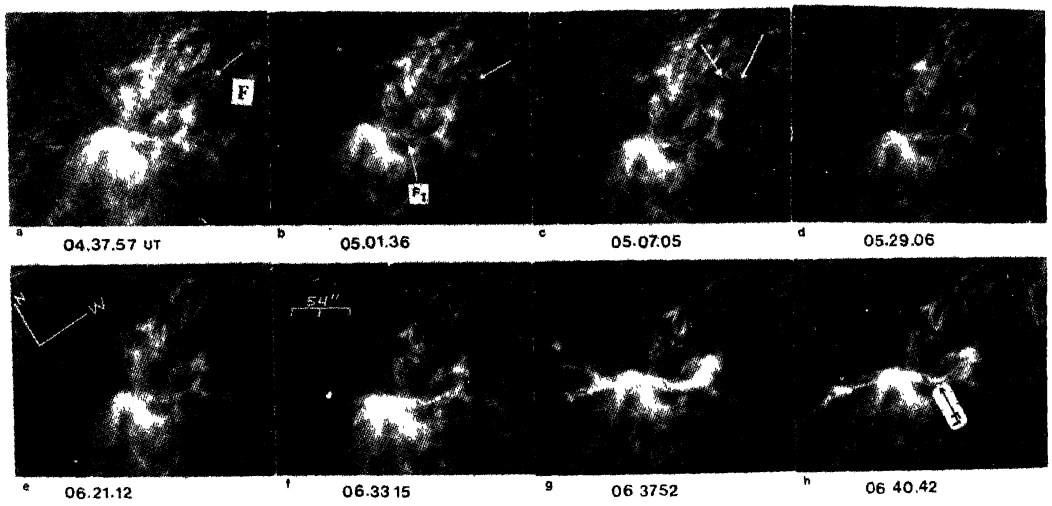

Figure 2. High resolution H-alpha filtergrams of April 3, 1980 flare occurred at 0630 UT of importance 1B in the same region 16740. Arrows show discrete dark material moving from north to south. Notice the activity in filament **F1**.

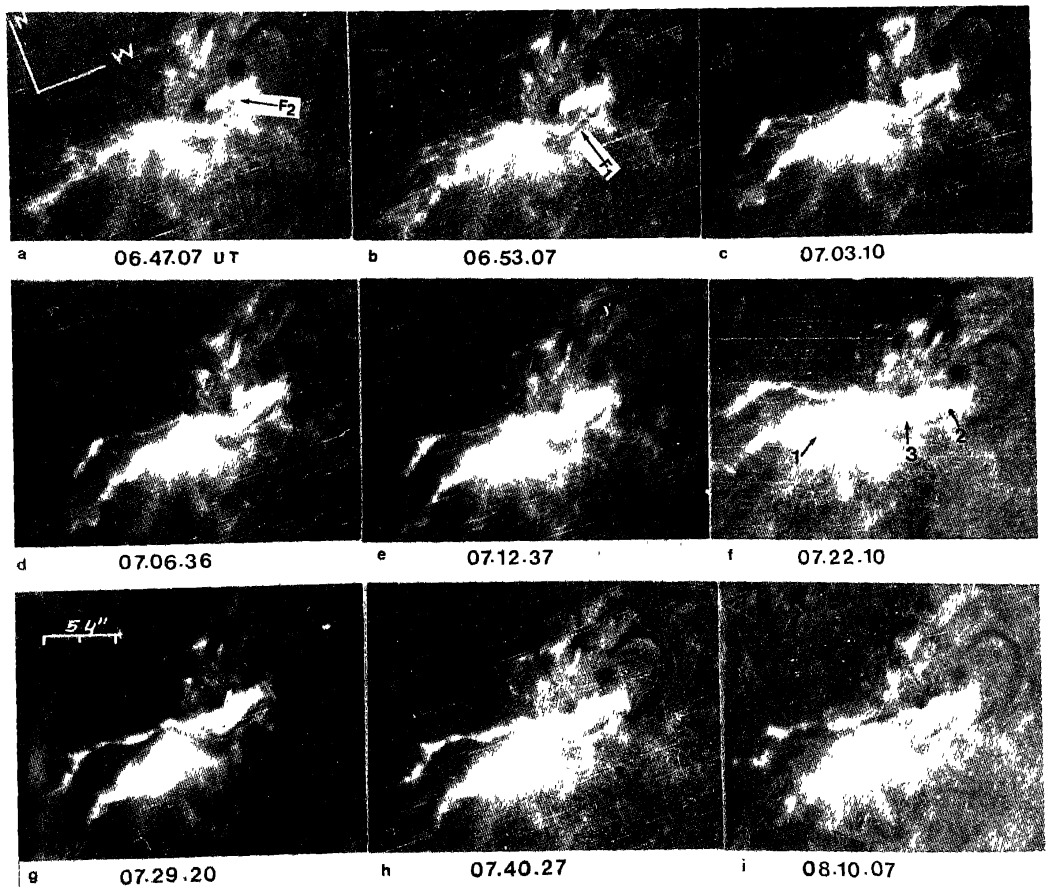

Figure 3. H_α high resolution filtergrams of April 3, 1980 showing development of two-ribbon flare (main flare) of importance 2B occurred in Hale region 16740. The identified flare kernels are grouped in pairs 1, 2 and 3 and marked on the filtergrams.

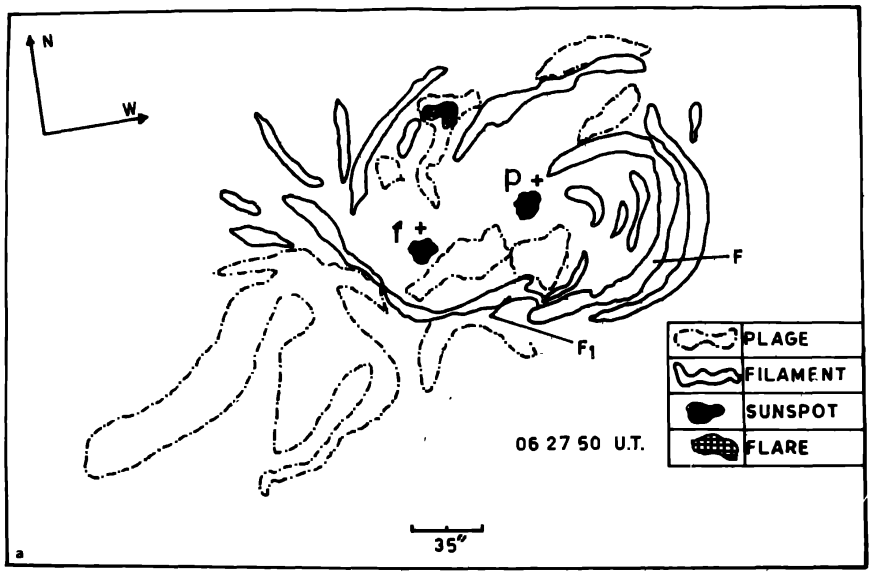

(a)

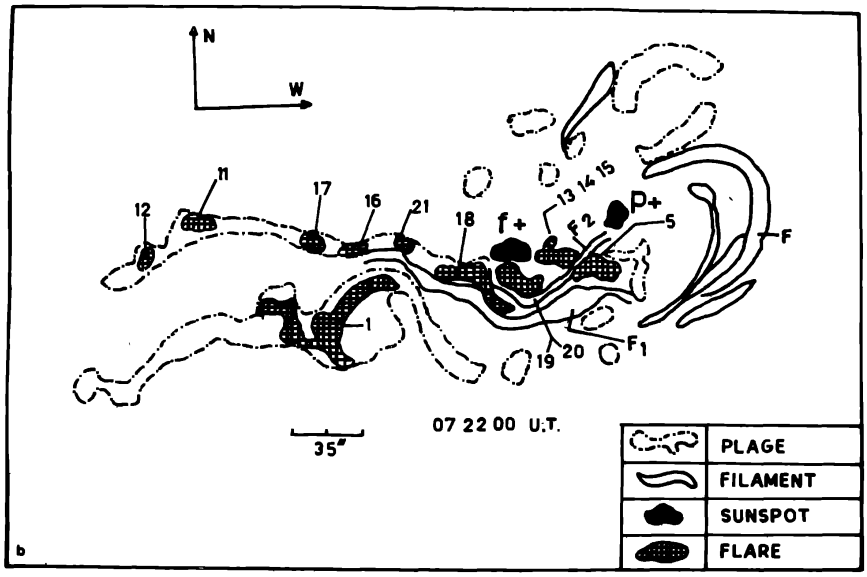

(b)

Figure 4. A line drawing of the H_α field of the Hale region 16740 on April 3, 1980 before (a) and after (b) the flare occurrence. Note the location of fine filaments **F1** and **F2.**

Reports no. 430, part I. A Superimposition of H_α flare kernels (hatched) and sunspots (dark) on the magnetogram, taking into consideration the 11 hrs delay is shown in figure 5. The superimposition indicated that inside the surrounding negative polarity, a strong positive field existed and many small regions of positive polarities appeared at the boundary of the negative polarity. As the magnetogram was taken 11 hrs after the flare, we cannot get an exact idea about the magnetic structure of the region during the flare, but this superimposition definitely implies that the flare occurred in magnetically complex region. The sunspot configuration in the region was changing since its appearance on the solar disk on 1980 March 26.

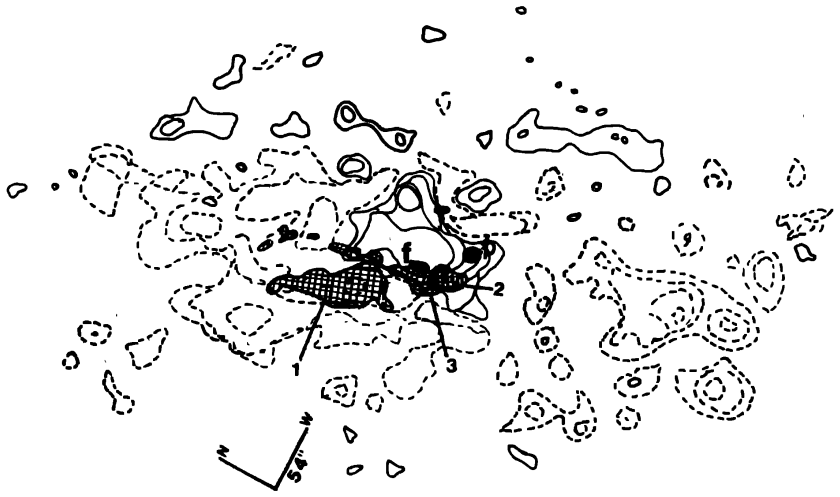

Figure 5. Superimposition of H_α flare kernels pairs on the Mt. Wilson magnetogram taken about 11 hrs after the flare. Note that flare kernels pair no. 3, occurred in strong magnetic field gradient. (see text).

2.1.2. Growth and separation of flare ribbons

The image scale of the H_α filtergrams, recorded on Kodak technical pan film no. 2415 was 44" arc per mm. The measured area of the various flare kernels forming the ribbons in millionths of solar disk is shown in figure 6 (bottom). The flare kernels 1 and 5 showed small growth around 0640 UT and after that they declined, however, the rise and decay both were rapid. The major flare started around 0650 UT when the kernel 1 showed huge growth during 0650 to 0710 UT. The flare kernel 1 peaked at 070915 UT in H-alpha. Around 0647 UT three new kernels 13, 14 and 15 appeared as shown in figure 4b. These kernels joined with kernel 5 around 0655 UT. Thus the area of the kernel 5 since 0655 UT is actually an integrated curve for 5, 13, 14 and 15. This curve shows two peaks at 065630 and 0713 UT. The flare kernels 18, 19 and 20 identified around 0702 UT appeared to join together at 0707 UT. The integrated area curve of these kernels showed it's maximum at 071930 UT. The growth and decay of all kernels were slow as inferred from area curves in figure 6.

We have measured the separation between opposite flare kernels as shown in figure 7 (left). This has been done to know whether all features forming a ribbon move with the same velocity. Further, to know whether each kernel shows motion or not, we have also measured the distance of the flare kernels from the following spot **f**, assuming that during the flare the spot was stationary. The distances of kernels 1, 5 and 19 from the following spot f are shown in figure 7 (right). The flare ribbon 1 which occurred in negative polarity, showed largest separation velocity of about 20 km s^{-1} during impulsive phase around 0700 UT. The velocity of the ribbon 1 decreased as it moved away from the spot **f** and finally stopped at 0735 UT. On the other hand flare kernels 5, 13, 14 and 15 did not show any motion. However, flare kernel 19, which formed a ribbon with kernels 18 and 20, showed motion but towards the following spot **f**. The leading edge of this ribbon (kernel 20) struck with the **f** spot around 0722 UT. The flare kernel 19 showed velocity of separation of about 8 km s^{-1}, in the beginning around 0705 UT. It was identified on the magnetogram in inverted positive polarity and in south-east to the spot **f**. Thus during expansion towards spot **f**, it was experiencing

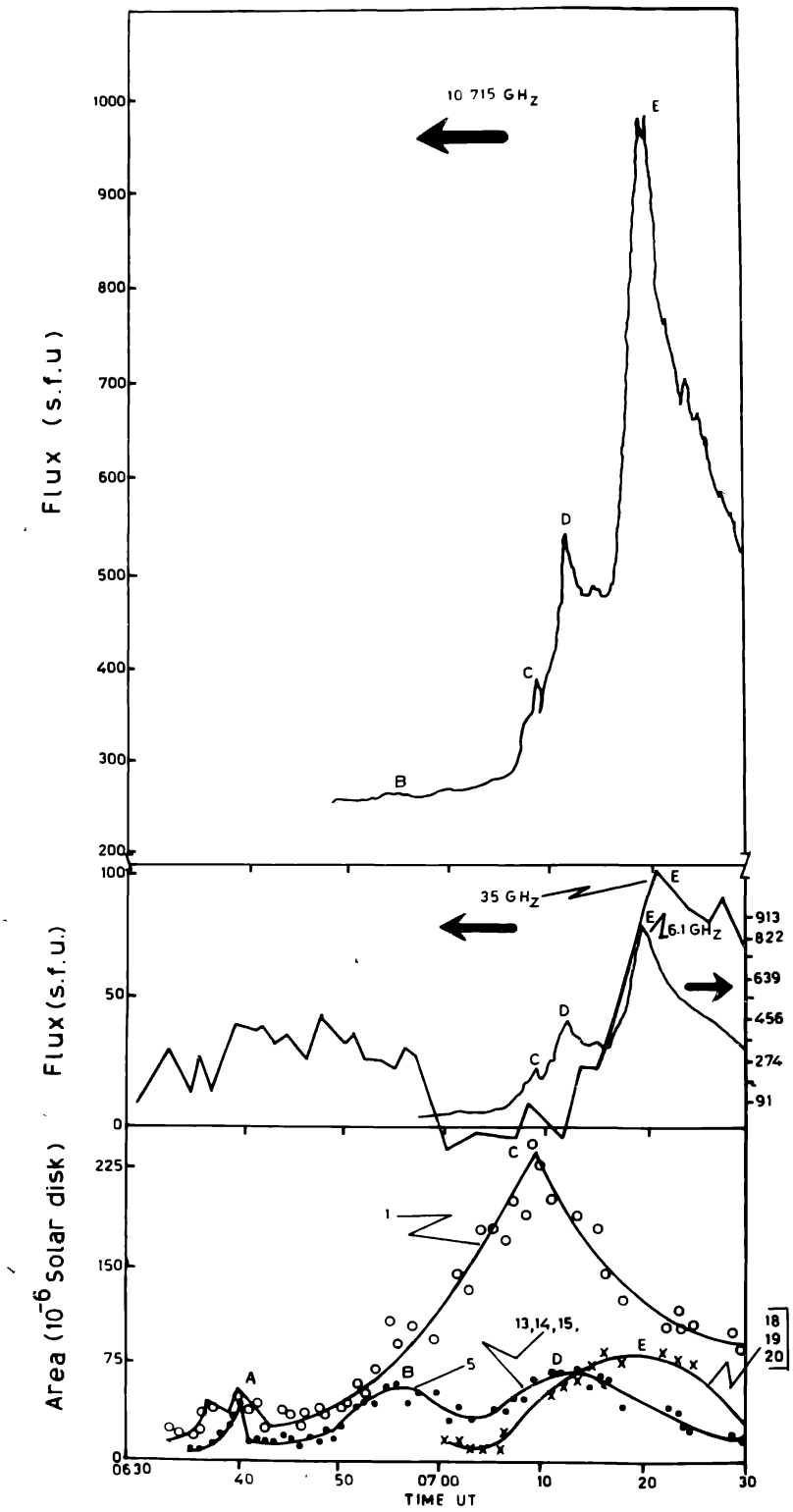

Figure 6. Time correspondance of H_α flare kernels and microwave flux enhancements. Bottom — H_α growth curve in terms of area of the flare kernels in millionth of the solar disc. Middle and top — microwave flux enhancement at 6.1, 10.715 and 35 GHz.

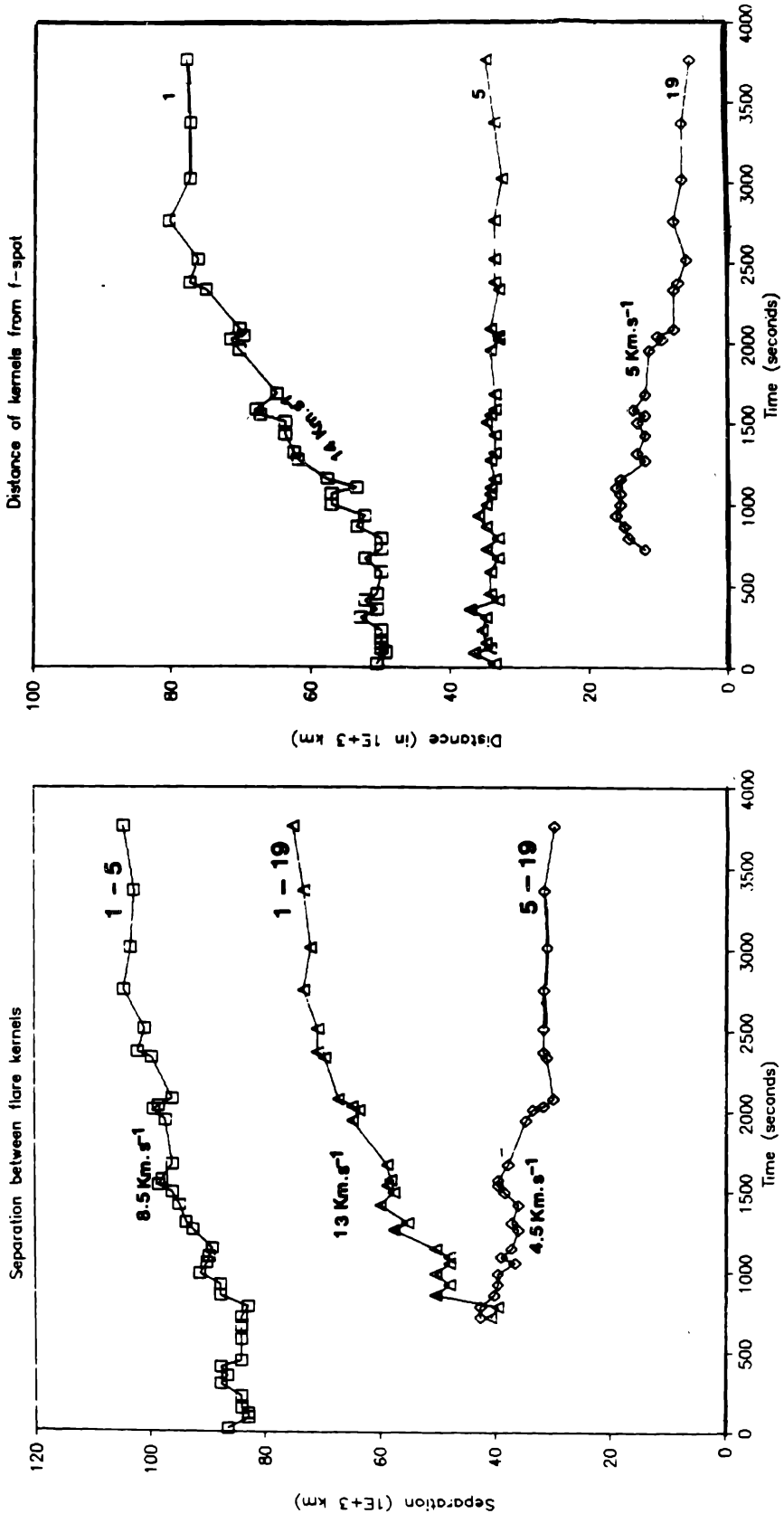

Figure 7. (a) Separation between opposite flare kernels. The separation velocity is marked on the curves. The time $t = 0$ is taken at 0650 UT. (b) Distance of flare kernels from the following spot f. The expansion velocities of kernels are marked on the curves. The time $t = 0$ is taken at 0650 UT.

strong magnetic field. The average velocities of separation between kernels and from spot f are marked on the curves shown in figure 7.

2.2. *Radio observations*

2.2.1. Microwave emission

In association to the flare under study, microwave (MW) emissions were observed at frequencies ranging from 1 GHz through 35 GHz. This indicates that the flare was a strong emitter of electrons originating from very deep in the solar atmosphere. The observations were obtained in eleven different frequencies from Toyokowa (1, 2, 3.75 and 9.4 GHz); Strahulung (3 and 9.5 GHz); PRL (2.7 GHz); Pulokov (6.1 GHz); Bern (10.4 GHz); Dwingeloo (10.715 GHz) and Nogoya (35 GHz) observatories.

In figure 6 (middle and top) are shown microwave bursts observed in association with optical flare in view of time correspondance. The MW bursts were observed on various frequencies as mentioned earlier, but in figure 6 we have shown flux enhancements in three selected frequencies (6.1, 10.715 and 35 GHz). However, in figure 8, we have shown intensity flux profiles observed in frequencies 1, 2, 3.75 and 9.4 GHz.

We have identified three different flux enhancement spike groups, C, D, and E, in view of time correspondance with various H_α flare kernels. The group C in all frequencies in figure 6 is associated with optical flare ribbon 1, the group D is associated with flare kernels 5, 13, 14 and 15 (now known as pair 2). The highest flux enhancement group E is associated with flare kernels 18, 19 and 20 (now known as pair 3). Now upon correlating in time the optical events with microwave emissions and in view of flare field topology (figures 4 and 5), we observe the following:

(i) The flare ribbon 1 formed in strong negative polarity, having greater area and expansion velocity but did not give rise to a strong microwave burst.

(ii) On the other hand pairs 2 and 3 which occurred in region of strong magnetic field gradients and whose H_α area was not as large as of ribbon 1, gave rise to higher flux enhancements D and E respectively.

The intensity profiles of MW bursts at 1, 2, 3.75 and 9.4 GHz (Toyokawa) shown in figure 8, reveal two interesting characteristic features as follows :

(i) At 070339 UT a strong burst of 150 sfu was observed in 1 GHz. This was reverse polarised (i.e. left handed). Following it, a complex structure in spikes was seen.

(ii) The MW bursts C, D and E were observed in all four frequencies but at 1 GHz and 2 GHz the burst groups were polarised in right sense (i.e. right handed) while at 3.75 and 9.4 GHz they were polarised reversely. This may indicate that there were two sources to generate strong microwave emissions and both were moving away from each other.

The microwave spectrum of each individual group is determined from flux versus time plots of various frequencies as mentioned earlier. The spectral evolution of each group is shown in figure 9. It is obvious from this figure that each individual group has two peaks, one at between 3 and 4 GHz and second at 10.5 GHz. The spectrum is steep above 10 GHz indicating emergence of higher energy radiations from the source during the 1st step acceleration. However, the spectrum of the second peak is very hard (> 2). The two peaks in the spectrum may either indicate that the two separate mechanisms were operating or double injection of energetic electrons at two different heights was taking place.

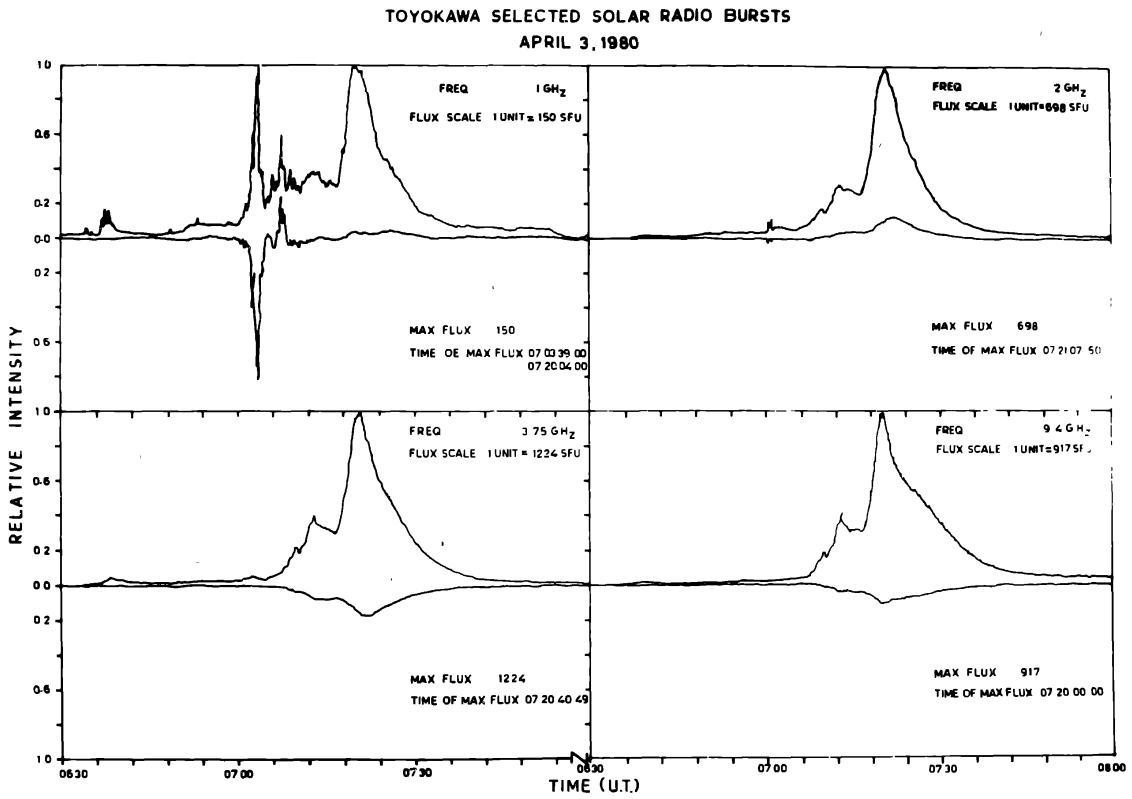

Figure 8. The Toyokawa intensity profiles of microwave bursts at 1, 2, 3.75 and 9.4 GHz. Note the reversal in polarisation of the MW burst groups C, D and E at frequencies 3.75 and 9.4 GHz.

2.2.2. Dynamic radio bursts

In association with the present flare, a type IV burst of intensity 2 from 0637-0735 and 0701-0735 UT was observed in decimetric and metric bands respectively. Also associated with the flare were metric band type II radio bursts of intensities 2 and 3 during 0706-0729 and 0716-0722 UT as reported by Culgoora and Weissenau Radio Observatories respectively.

2.3. *X-ray observations*

2.3.1. Hard X-ray emissions

The hard X-ray bursts in association with the flare under study was detected with the HXRBS on the SMM. During 0636-0642 UT a minor hard X-ray burst occurred with a peak count rate of 340 c/s at 0638 UT. This burst appears to be associated with the flare at 0637 UT occurred before the main TR-flare. However the major hard X-ray burst started when the SMM was in the night. Thus the spikes, if any, in association with the maximum in H-alpha at 0709 and 0713 UT could not be detected. Nevertheless, SMM again appeared before the sun as shown in figure 10, at 071730 UT and thus could detect a major burst with a peak rate of 1700 c/s at 071905 UT, obviously associated in time with H_α peak of pair 3 constituted from kernels 18, 19 and 20.

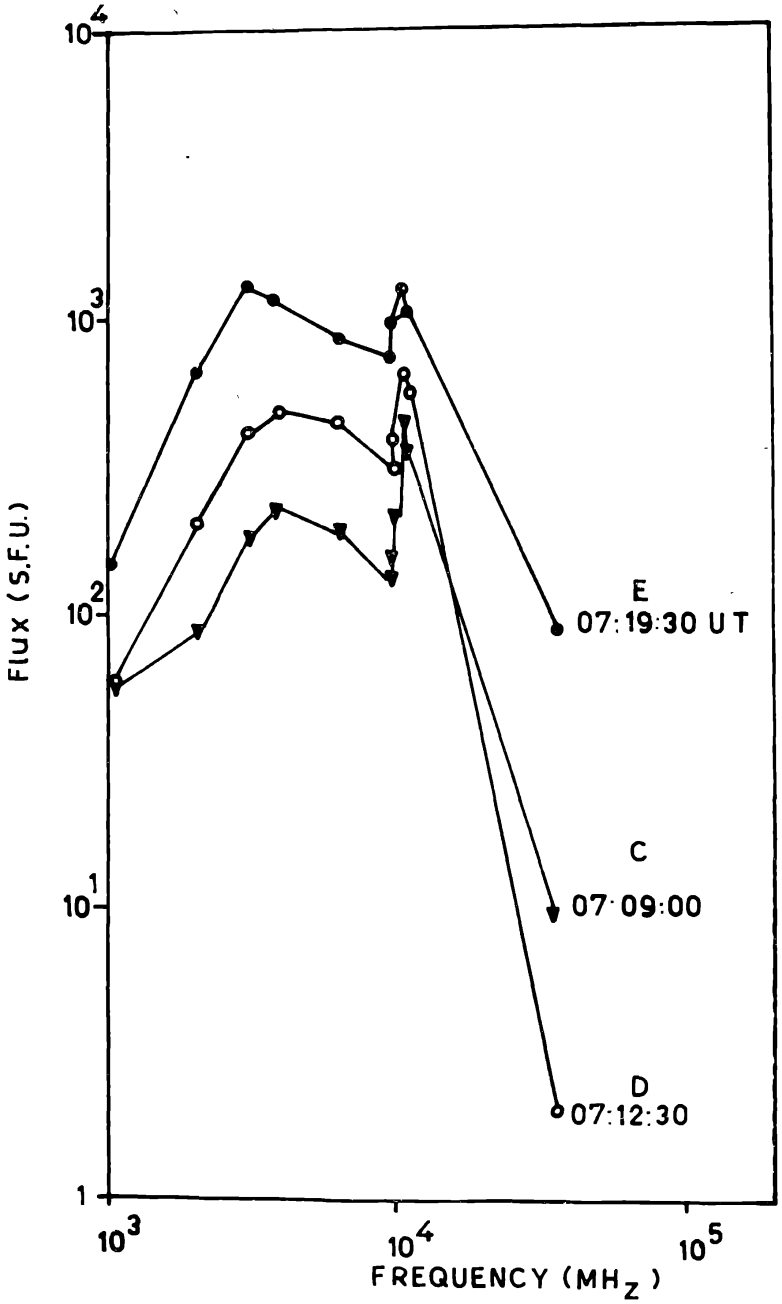

Figure 9. The spectral evolution of the microwave bursts C, D and E showing variation of flux over frequencies. The two peaks in the curves are obviously seen.

2.3.2. Soft X-ray emission

This flare has been reported as an M2 flare with a duration of 4 hrs (Sheeley *et al.* 1984). We have estimated the flux at 071930 UT in 0.5-4A and 1-8A of about 2.8×10^{-6} WM^{-2} and 2.9×10^{-5} WM^{-2} respectively.

3. Energetics and dynamics

3.1. *Estimation of H-alpha energy release*

The total energy radiated in H_α by a flare during it's duration t (in seconds) is given by

$$E_{H_\alpha} = 1/3\,\Delta E_{H_\alpha} . t \text{ ergs} \quad \ldots (1)$$

where ΔE_{H_α} according to Thomas (1970), is the energy released in H_α per second and determined by photometry of the whole flare area as follows :

$$\Delta E_{H_\alpha} = 7.9 \times 10^{33} \bar{A} \left(3.1 \frac{P_0(H_\alpha)}{P_0(C)} - 1 \right) \text{ ergs s}^{-1} \quad \ldots (2)$$

where $\bar{A}$ is the area of flare in steradians and $P_0(H_\alpha)/P_0(C)$ is the value of peak intensity with respect to the continuum at the disc center. The total area and duration of the present flare were determined as 6.6×10^{-8} steradians and 6×10^3 seconds respectively. The value determined for $P_0(H_\alpha)/P_0(C)$ was 1.2 for this flare of importance 2B. We have estimated a total H_α energy release of about 2.8×10^{30} ergs.

3.2. *Soft X-ray thermal emission*

The energetics of the SXR emitting source may be estimated from the formula recently given by Starr *et al.* (1987), as following :

$$k . T_{eff} . EM(\text{SXR}) = n . U_{therm} (\text{SXR}) \quad \ldots (3)$$

where k is Boltzman constant, T_{eff}, EM and n are effective temperature, emission measure and electron density of the source and U_{therm} is the total thermal energy content of the source plasma. The effective colour temperature and corresponding emission measure were estimated from GOES observations by the ratio technique described in Thomas, Starr & Crannell (1985). In this procedure, the effective colour temperature is defined to be the temperature of an isothermal plasma which would produce the observed ratio of responses in the two GOES detectors. The estimated values of T_{eff} and EM (SXR) at 071930 UT were 9.5×10^6 °K and 4.67×10^{49} cm^{-3} respectively. On putting these values in equation (3), we obtained $n.U_{therm} \approx 6.1 \times 10^{40}$ ergs cm^{-3}.

Measurements of the energy emitted by flares in H_α have been shown by Thomas & Teske (1971) to be proportional to the soft X-ray emissions and to depend on flare importance number. Thus assuming that thermal energy emitted by SXR source is as much as energy released in H_α i.e. 2.8×10^{30} ergs, we find, upon putting this value against U_{therm} in above estimation of SXR source energetics, electron density (n) at the flare peak time of about 2.17×10^{10} cm^{-3}.

3.3. *Hard X-ray thermal emission*

The thermal energy content of the flaring HXR source, assuming isothermal emission measure, can be expressed as (Starr *et al.* 1987) :

$$U_{\text{therm}}\,(\text{HXR}) = (nV)\, k\, .\, T_{\text{eff}}. \qquad \ldots (4)$$

We have already determined electron density n as 2.17×10^{10} cm^{-3} at peak time. We used the same electron density in computing U_{therm} (HXR). Though the sizes of H_α and HXR sources are generally not the same but, presently, the volume V of HXR source has been determined from volume of H_α kernels in pair 3 (18, 19 and 20) assuming same sizes for both because on time correspondance these kernels have been identified as feet of the source for strong MW and HXR emissions. We measured the size (w) of the kernels and found it to be about 18 arc sec. The distance between two kernels ($2L$) was about 43 arc sec. If we assume the circular geometry of the loop, the volume, L^2w is estimated to be 2.85×10^{27} cm. The temperature T is estimated about 4.4×10^8 k (38 KeV) as discussed in next section 3.4. On putting all values, we find U_{therm} (HXR) $\simeq 3.8 \times 10^{30}$ ergs.

However, our estimation involves an over simplified view of the burst geometry and thus it contributes as much as a factor of two to the rms scatter in the calculated energy content of the HXR source. In equation (4), the emitting volume may also be estimated from a length (L) determined from the plasma's ion sound speed (C_s) and the measured rise time (t_r) of the burst (Batchelor *et al.* 1985) as follows :

$$V = L^3 \qquad \ldots (5)$$

$$L = C_s t_r \qquad \ldots (6)$$

$$C_s = (kT_e / m_i)^{1/2} \qquad \ldots (7)$$

where m_i is the average ion mass (taken to be the proton mass). Assuming T_{eff} and T_e were the same, equation (4) can be written as

$$EM\ (\text{HXR}) = \frac{\left[U_{\text{therm}}\,(\text{HXR})\right]^2}{\left[kT_{\text{eff}}\right]^{7/2} t_r^{\,3} m_i^{-3/2}}. \qquad \ldots (8)$$

Th temperature T_{eff} is estimated about 4.4×10^8 K as discussed in next section 3.4 from the data published by Wiehl *et al.* (1985). The t_r is about 95 seconds. Putting U_{therm} (HXR) $\simeq 3.8 \times 10^{30}$ ergs, we obtained EM (HXR) $\simeq 1.33 \times 10^{44}$ cm^{-3}.

3.4. *Hard X-ray non-thermal emission*

The hard X-ray burst emission with a power-law spectrum can be produced by a beam of electrons whose energy distribution is itself in the form of a power law (non-Maxwellian and therefore "nonthermal"). However, the energy lost by the beam electrons depends on the nature of the target that they encounter when producing the observed bremsstrahlung X-rays. Two extreme possibilities are the thin target and thick target cases. In either case, if the observed X-ray photon spectrum is in the form of a power-law, it can be written as :

$$\frac{dN\,(E_p)}{dE_p} = A\left(E_p/E_m\right)^{-\gamma} \text{ photons cm}^{-2}\,\text{s}^{-1}\,\text{KeV}^{-1} \qquad \ldots (9)$$

where E_p is the photon energy in KeV, and E_m is a 'mean' energy also in KeV. In our present event, we have taken the value of E_m to be 50 KeV.

Shown in figure 10, obtained from Dennis (private communication), is evolution of hard X-ray flux and spectrum for 1980 April 3, event under study. The top panel shows the time profile of the HXRBS total count rate in 27-420 KeV. The middle and the bottom panels show the evolution of A, 50 KeV flux, and, γ the special index respectively.

The rate at which electrons of various energies from the exciting beam enter into the X-ray emitting target region can be expressed in a similar form as a photon spectrum :

$$I(E_e) = B_1 E_e^{-B_2} \text{ electrons s}^{-1} \text{ KeV}^{-1} \quad \ldots (10)$$

where E_e is the electron energy in KeV and B_1 and B_2 are spectral parameters. For the case of thick target emission, the electron beam spectral parameters can be found from those defining the observed X-ray photon spectrum by means of the following relationships (Starr *et al.* 1987) :

$$B_2 = \gamma + 1 \quad \ldots (11)$$

and

$$B_1 = 3 \times 10^{33} A E_m^{\gamma} \gamma (\gamma - 1)^2 b(\gamma - {}^1/_2, {}^1/_2) \quad \ldots (12)$$

where $b(m, n)$ is the beta function. The time dependent flux of energy into the target due to electrons with kinetic energies above a threshold energy E_0 can thus be expressed by the following relation derived by Hoyng *et al.* (1976)

$$P(E_0) = 5 \times 10^{24} A E_m^{\gamma} \gamma (\gamma - 1)\, b\, (\gamma - {}^1/_2, {}^1/_2)\, E_0^{-\gamma+1}. \quad \ldots (13)$$

Choosing $E_0 = 25$ KeV, we find $P_{25} \simeq 10^{28}$ erg s^{-1} and corresponding beam strength of electrons above 25 KeV i.e. $F_{25} \simeq 2.5 \times 10^{35}$ s^{-1}. P_{25} is the energy per second entering into the X-ray emitting target region in the form of nonthermal electrons with energies above 25 KeV. The total energy in the electron beam can, therefore, be calculated by integrating over the duration. The duration of the HXR burst observed in association to pair no. 3 in H_α was around 350 seconds. This gives total energy in the electron beam i.e. $U_{beam} \simeq \int P_{25}\, dt \simeq 3.5 \times 10^{30}$ ergs. Incidentally it is almost same as calculated by assuming the thermal origin of HXR, in the previous section. Thus it appears that the present event can be explained by both thermal and non-thermal incidence. This kind of explanation has been given earlier by Wiehl *et al.* (1985). In figure 11, we have shown hard X-ray spectra at the time of maximum MW emission intensity, for both power-law and thermal assumptions of the incident spectra.

The thermal bremsstrahlung function shown in figure 11, used to calculate incident flux is as following (Wiehl *et al.* 1985)

$$I(E) = K_T E^{-1} T^{-0.5} G_E \exp\,[-(E - 50)/T] \quad \ldots (14)$$

where K_T and T are the fitting parameters, E is the photon energy in KeV, T is the temperature in KeV and $I(E)$ is the X-ray flux in photons cm^{-2} s^{-1} KeV^{-1}. The total effective Gaunt factor,

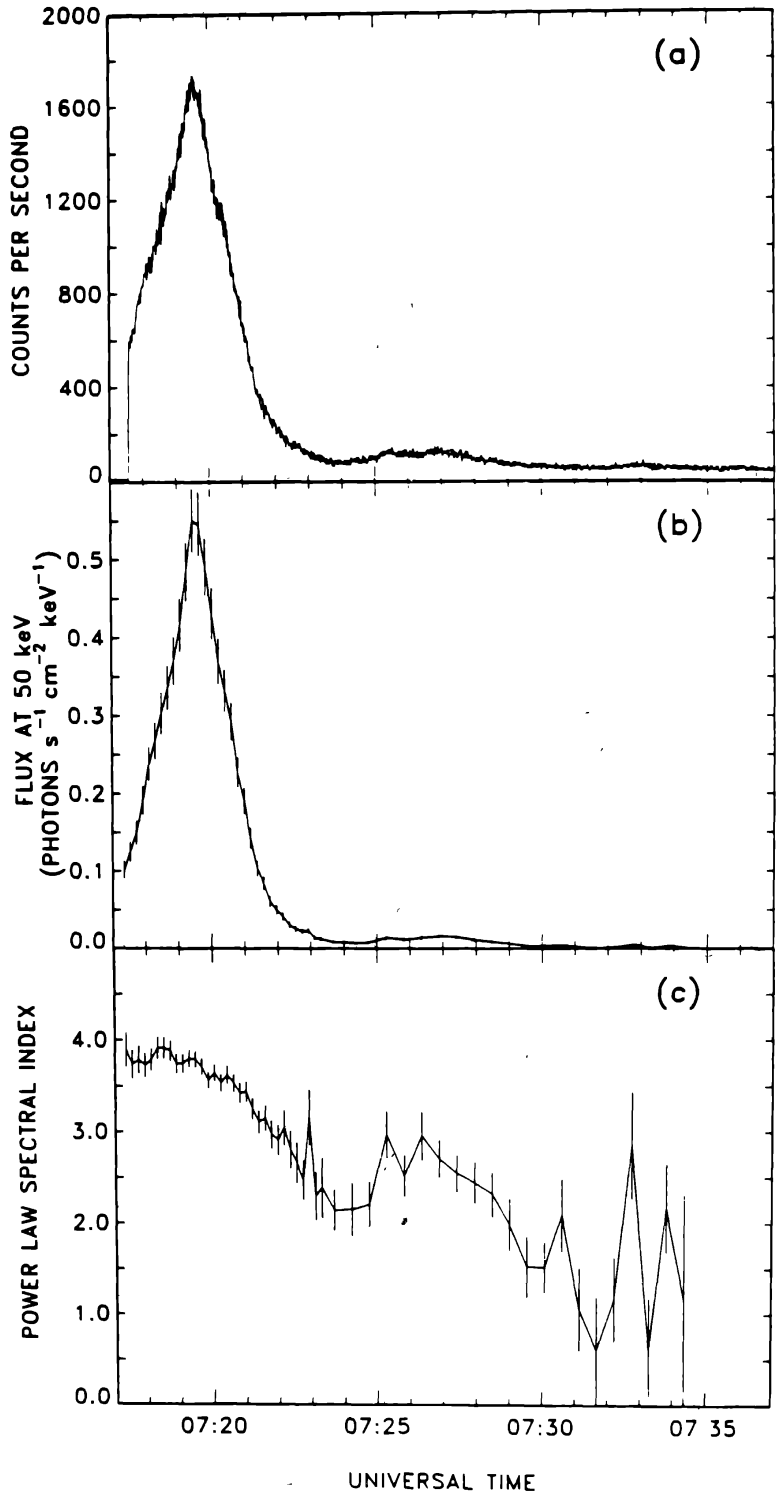

Figure 10. The evolution of hard X-ray flux (courtesy B. Dennis, GSFC, USA) Top—time profile of HXRBS count rate in 27-420 KeV. Middle—evolution of A (50 KeV flux). Bottom—evolution of γ (spectral index).

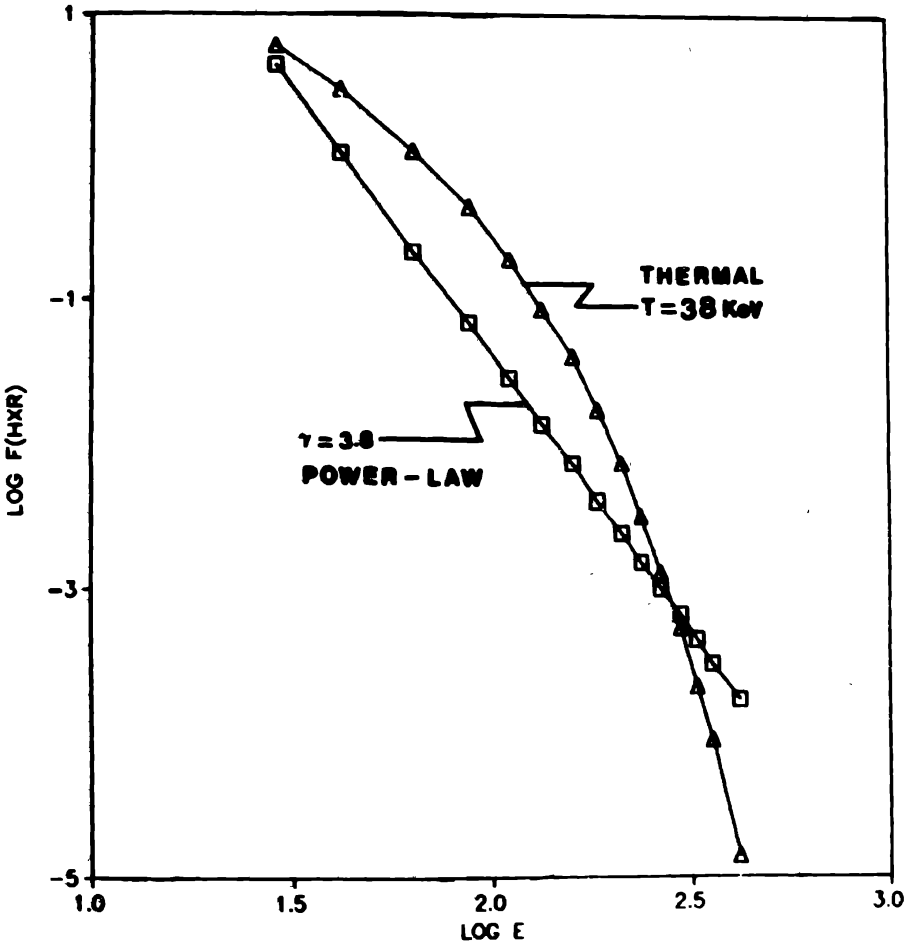

Figure 11. The hard X-ray spectra of the flare kernel pair no. 3 at the time of maximum i.e. 071905 UT, assuming both power-law and thermal incident spetra. The horizontal scale is energy, E in KeV, and vertical scale is flux, F in photons cm^{-2} s^{-1} KeV^{-1}. The flux is determined at the mean energy of each channel detectors.

Ge $(-Gz^2)$ was determined for $T \simeq 38$ KeV. The thermal emission measure can be calculated from T and K_T as follows :

$$EM = 9.3 \times 10^{41} K_T \exp(50/T) \text{ cm}^{-3}. \quad \ldots (15)$$

The temperature T was determined from figure 12, which is a curve drawn between photon spectral index γ from nonthermal incidence and temperature T from thermal incidence. The data points for this curve have been taken from Wiehl *et al.* (1985), where they have analysed 13 great MW bursts and hard X-rays from solar flares assuming each event can be explained by both thermal and nonthermal incidence. However, we have shown in next section that temperature T (38 KeV) derived from figure 12, as we know γ for the present event, is in good agreement with that derived from MW spectral analysis.

3.5. *Microwave emission*

Under the assumption that both HXR and MW emissions originated in a common single temperature region, we can estimate at the peak time, the area of the MW source and the magnetic field strength in the source. In order to determine the area, we first consider the

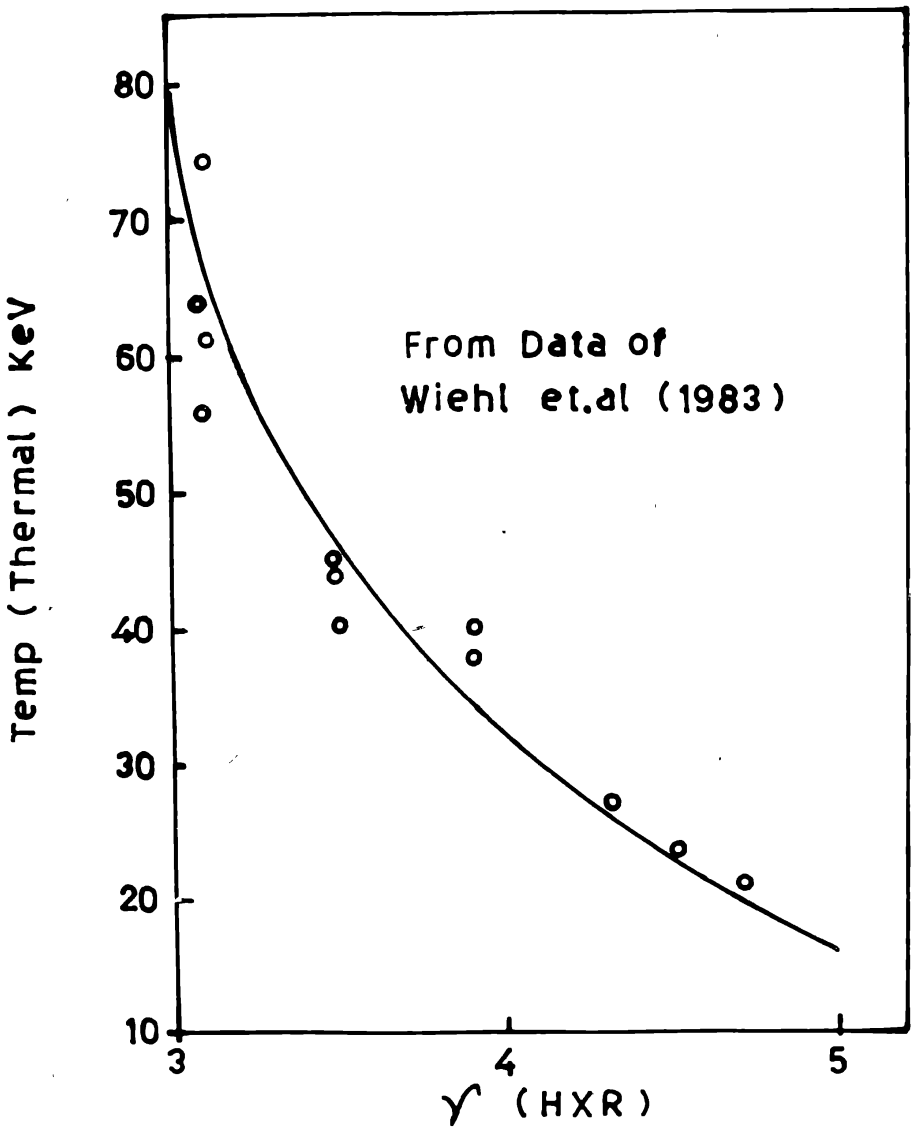

Figure 12. A curve between photon spectral index γ from non-thermal incidence and temperature T from thermal incidence (data points from Wiehl *et al.* 1985). For details see text.

microwave spectrum at frequencies $\leq f_{peak}$. The microwave source is generally believed to be optically thick in this range, and the spectrum for a uniform single temperature source is given by the relation from Crannell *et al.* (1978)

$$S = 0.16\, f^2\, AT. \qquad \ldots (16)$$

In this relation S is microwave flux in sfu, f is frequency in GHz, A is area in 10^{18} cm^2 and T is temperature in KeV. For the present, we assume that the flux S_{peak} at f_{peak} is dominated by such a single temperature source. Further our assumption that a common population of electrons is responsible for both HXR and MW allows us to substitute the temperature derived from the X-ray spectrum in section 3.4. The area A_{peak} can then be calculated by substituting values for S_{peak} = 1220 sfu; f_{peak} = 10.4 GHz and T = 38 KeV in relation (16), we find $A_{peak} = 1.9 \times 10^{18}$ cm^2.

The area A_{peak}, determined from equation (16), may not be identically equal to the actual area of the loop. A given arch, if viewed from the side, has a projected area of $2Lw$, where L is the half-length of the loop and w the width of the loop.

As mentioned earlier in section 2, strong MW and HXR emissions had been observed in association with the flare kernels in pair 3. We measured the size of the kernels and found it about 18 arc sec. It was also observed that pair 2 and pair 3 were feet of the loop. The size of the kernels in pair 2 was also about 18 arc sec. The distance between the two pairs was about 43 arc sec. If we assume a circular geometry of the loop, then $2L$ = 43" and taking w = 18", area of this H_α loop would be, $2Lw \simeq 3.8 \times 10^{18}$ cm^2. Incidentally, this is almost equal to A_{peak} determined by relation (16), if we consider contribution from only one pair of kernels i.e. pair no. 3 and thus half of 3.8×10^{18} cm^2. This emphasizes that H_α kernels in pairs 2 and 3 are true feet of active loops and thus our estimation of $T \simeq 38$ KeV also is in good approximation. However, it appears that the conduction front moving along the loop was predominantly from pair 3, because strong MW and HXR emissions were found to be associated with it. Further, from the above result our assumption of single temperature source (common source) for MW and HXR appears to be good as estimated area from their spectrum i.e. A_{peak} is in good agreement with that estimated from H-alpha observations.

The magnetic field strength was determined using the following expression for f_{peak} obtained from Dulk & Marsh (1982).

$$f_{peak} = 4.9 \times 10^{-3} (nl)^{0.1} (\sin \theta)^{0.6} T^{0.7} B^{0.9} \quad \ldots (17)$$

where θ is the angle between the magnetic field and the line of sight, l the characteristic length of the source in units of 10^8 cm (here $l = 12.6 \times 10^8$ cm); T the temperature in KeV estimated from HXR and MW spectrum. For $\theta = 60°$, we obtained $B \simeq 140$ G, which is in good agreement with the earlier results obtained by Wiehl *et al.* (1985) and Kosugi *et al.* (1988).

The total thermal energy of the flare plasma at $t_{\mu max}$ is calculated from the following expression under the assumption that the ions and electrons have the same temperature and number density

$$U = 2 \times 10^{-3} r^3_{peak} nT \quad \ldots (18)$$

where r_{peak} is radius of the source. On putting $r_{peak} = 6.3 \times 10^8$ cm, we obtained $U \simeq 4.1 \times 10^{30}$ ergs.

4. Discussion

The H_α observations of energetic two-ribbon flare of 1980 April 3, have been analysed in detail because the spatially resolved data for this important event might reveal a clue to the condition that allow a particular flare to be the site for release of very high energy observed as MW and HXR emissions.

It is obvious from the field configuration (figure 4) and magnetogram (figure 5) that the region was complex in nature in the sense that the polarities were intermingled. From figure 4 it appears that either (i) flare kernel 5 was one foot of an invisible loop and the foot

on the other side was of kernels 13, 14 and 15 of complex loop structure and this loop structure perhaps did not have any expansion as we could not see any motion of these kernels. Further, on the other hand a loop was formed by kernel 18 on one side and 19 and 20 on the other side. Or else (ii) the kernels in pair 2 were feet on one side of a loop structure and kernels in pair 3 were feet on the other side. However, it is true that a complex loop system was existing. The kernels 19 and 20 touched to the following spot f around 0722 UT during their expansion.

The peaks in the hard X-ray bursts and the power of the energy released into fast electrons depends on how close the corresponding H_α brightening is to the sunspot umbra (Dwivedi *et al.* 1984; McCabe 1985). The hard X-ray and MW bursts (E) peaked around the same time indicating that the source for these bursts were H_α flare kernels 18, 19 and 20. The 35 GHz MW burst peaked around 0722 UT when flare kernels 19 and/or 20 entered into the penumbra of the following spot f. However, observed delays between H_α flare kernels and the corresponding microwave bursts may be explained as different mechanisms of energy transport might operate as suggested by Kampfer and Magun (1983). We have also drawn similar conclusion, that several sources or acceleration sites were existing and at least two different mechanisms were operating for energy transport in the flare of 1980 April 3. The basis for these conclusions is, as mentioned earlier in section 2.2.1, that there were two sources and both were moving away from each other. The sources were in the beginning at a height corresponding to frequencies of about 3.75 and 10 GHz. Further, the two peaks in the spectrum may indicate that either two separate mechanisms were operating or double injection of energetic electrons at two different heights was taking place. Further, it is important to note that these two peaking frequencies are close to those frequencies where reverse polarisation was observed.

Further, the two peaks in the MW-spectral evolution may be explained from the fact that simultaneous and multiple reconnections were taking place between the flux tubes at two different heights or levels in the solar atmosphere causing interaction of loops. The visual inspection of field topology (figure 4b) shows that magnetic field gradient is different for different pairs of kernels. However it was unambiguously higher for pair 3 as compared to ribbon 1 and pair 2. The higher magnetic field gradient will give rise to higher energy electrons and thus will be observed at higher frequencies, while lower magnetic field gradient reconnection site will produce low energy electrons and being observed at low frequencies.

It is shown that the present event may be explained by both thermal and non-thermal incidence of electrons. Further, our assumption of common population of electrons for generating MW and HXR emissions is also found to be in good agreement with the determined energetics and dynamics of the flare kernels in pair no. 3. This means that for both emissions the thermal source was common. However, when we assume that the non-thermal incidence is responsible for both MW and HXR emissions, then it would be of interest to know which model explains the present event in view of the results obtained in our analysis. The present flare as a whole may be classified as an extended flare according to its characteristics described by Kosugi, Dennis & Kai (1988). Thus, according to them, the flare must have been produced by electrons trapped in the coronal magnetic loop. They concluded that precipitating electrons give rise to impulsive flares. However, the two types of flares may be two opposite extremes and the actual situation for a few kernels within a large flare may be a complicated one, as it appears in the present case as follows :

If we consider the pair no. 3 as an extended flare and due to non-thermal emissions by electrons trapped in coronal loop, we obtain the magnetic field strength $B \simeq 250$G. However by considering it an impulsive flare due to non-thermal electrons precipitated into the lower corona and the chromosphere, we get $B \simeq 425$G. We used these values to determine f_H and hence f_{peak}/f_H. In non-thermal model, we utilise the hard X-ray spectrum to estimate the electron energy spectral index (or the effective power-law index) δ as $\delta = \gamma + 1.5$ in impulsive flares (or thick target case) and $\delta = \gamma - 0.5$ for extended flares (or thin target cases), where γ is again the X-ray photon spectral index. However, we applied thick target and thin target case of X-ray production in both coronal trap and precipitation models and determined the effective temperature as follows (Dulk & Dennis 1982) :

$$T_{eff} = 2.2 \times 10^9 \times 10^{-0.31\delta} \times (\sin\theta)^{-0.36-0.06\delta} \times \left(\frac{f_{peak}}{f_H}\right)^{0.50+0.085\delta} \quad \ldots (19)$$

We obtained in coronal trap model,

$T_{eff} \simeq 1.3 \times 10^9$ °K or 112 KeV for thick target

$T_{eff} \simeq 2.0 \times 10^9$ °K or 172.4 KeV for thin target

and in precipitation model,

$T_{eff} \simeq 5.1 \times 10^8$ °K or 39.0 KeV for thick target

$T_{eff} \simeq 1.13 \times 10^9$ °K or 97.5 KeV for thin target.

The above determinations of the T_{eff} clearly show that the phenomenon of pair no. 3 in conjunction with the production of MW and HXR was a case of thick target from the electrons precipitated in lower corona and chromosphere, because in this case $T_{eff} \simeq 39$ KeV is in good agreement with earlier estimation of 38 KeV and used for various analysis in section 3. But it is also well established that in extended flares, microwaves are mainly emitted by MeV electrons which are trapped in a coronal loop or loops. Thus in the present event possibility of coronal trap model also exists, rather it may be a case of trap-plus-precipitation model as earlier suggested by Melrose and Brown (1976) and recently supported by Kosugi, Dennis & Kai (1988).

The present flare was associated with a coronal transient of a classic bright loop and centered at a position angle N80 on the east limb and had a latitudinal spread of 30° on each side of centre (Sheely 1984). It is estimated that pair no. 3 appeared at 070145 UT generated a shock which produced type II burst observed at 0706 UT. The time difference between beginning of these two events is, therefore, 255s. The location of the H_α flare kernels, pair no. 3, is W20, while the burst source was identified at W90. Thus, the shock travelled a distance of about 540,000 km in 255s. This allows us to estimate the velocity of the shock, V_{shock}, to be about 2118 km s^{-1}. The type II bursts are usually interpreted as originating in weak shocks, of magnetic Mach number $M < 2$ (Smerd, Sheriden & Stewart 1975). For the present event if we assume $M = 2$ then, Alfvén velocity, $V_a = 1054$ km s^{-1} which is very close to the speed of coronal mass ejection ($V_c = 1100$ km s^{-1}) observed at 0710 UT. This suggests that our estimation of association of coronal transient with H_α flare pair no. 3 is correct. With the help of Alfvén velocity determined above and found to be the velocity of the coronal transient, we estimated the magnetic field strength at a distance $2R$ from the disc

centre, as B = 2.9 G, a value which falls well within the range of magnetic field strengths (1.0-10.0 G) derived from radio observations at $2R$ from the disc centre by Dulk & McLean (1978) and by optical observations by Jain, Bhatnagar & Shelke (1984). It appears that type IV radio burst occurred at 0637 UT was perhaps associated with bright mass ejection observed at 0632 UT.

Acknowledgements

The author wishes to express his hearty thanks to Prof A. Bhatnagar for his keen interest in this work and encouragement. He is very thankful to Drs B. R. Dennis, C. Slottje, A. Magun, S. Enome, K. I. Kawabata, M. N. Gnevyshev, H. Auras and R. V. Bhonsle for providing HXR and MW data and to Prof. S. I. Gopasyuk and Prof. L. Dezso for white light observations for this study. Author would like to acknowledge many useful discussions with Drs R. R. Rausaria, R. K. Shevgaonkar, S. S. Degaonkar and B. N. Dwivedi. The author is also thankful to Dr A. Ambastha for reading manuscript critically as well as providing help in some computations. He also gives thanks to Mr L. L. Suthar for making good prints for this paper.

References

Batchelor D. A., Crannell C. J., Wiehl H. J., Magun A., 1985, ApJ, 295, 258.
Crannell C. J., Frost K. J., Matzler C., Ohki K., and Saba J. L., 1978, ApJ, 223, 620.
De Jager C., 1975, Solar Phys., 40, 133.
Dulk G. A., McLean D. J., 1978, Solar Phys., 57, 279.
Dulk G. A., Marsh K. A., 1982, ApJ, 259, 350.
Dulk G. A., Dennis B. R., 1982, ApJ, 260, 875.
Dwivedi, B. N., Hudson H. S., Kene S. R., Svestaka Z., 1984, Solar Phys., 90, 331.
Hoyng P., Brown J. C., Van Beek H. F., 1976, Solar Phys., 48, 197.
Hoyng P., Duijveman A, Machado M. E., Rust D.M., Svestka Z., Boelee A., De. Jager C., Frost K. J., Lafleur H., Simnett G. M., Van Beek H. F., Woodgate B. E., 1981, ApJ, 246, 155.
Jain R., 1983, Ph.D. Thesis, Gujrat University, India.
Jain R., Bhatnagar A., Shelke R. N., 1984, JA&A, 5, 323.
Jain R., 1985, BASI, 13, 253.
Jain R., 1986, MNRAS, 223, 877.
Kampfer N., Magun A., 1983, ApJ, 274, 910.
Kosugi T., Dennis B. R., Kai K., 1988, ApJ, 324, 1118.
Martin S. F., 1979, Solar Phys., 64, 165.
McCabe M. K., 1985, Solar Phys., 98, 127.
Melrose D. B., Brown J. C., 1976, MNRAS, 176, 15.
Neidig D F., 1978, Solar Phys., 57, 385.
Sheeley N. R. Jr., Stwart R. T., Robinson R. D., Howard R. A., Koomen M. J., Michels D. J., 1984, ApJ, 279, 839.
Smerd S. F., Sheridan K. V., Stewart R. T., 1975, Ap. Lett., 16, 23.
Starr R., Hevidl W. A., Crannell C. J., Thomas R. J., Batchelor D. A., Magun A., 1987, NASA Technical Memorandum 87816.
Svestka Z., 1976, Solar Flares, D. Reidel.
Svestka Z., Simon P., 1969, Solar Phys., 10, 3.
Thomas R. J., 1970, Doctoral Dissertation, University of Michigan, USA.
Thomas R. J., Teske R. G., 1971, Solar Phys., 16, 431.
Thomas, R. J., Star, R., Crannell C. J., 1985, Solar Phys., 95, 323.
Valnicek B., 1961, Bull. Astrn. Inst. Czech., 12, 237.
Wiehl H. J., Batchelor D. A., Crannell C. J., Dennis B. R., Price P. N., Magun A., 1985, Solar Phys., 96, 339.